Mass Spectral Evidence That Small Changes in Composition Caused by Oxidative Aging Processes Alter Aerosol CCN Properties

J. E. Shilling,[†] S. M. King,[†] M. Mochida,[†,‡] D. R. Worsnop,[§] and S. T. Martin*,[†]

School of Engineering and Applied Sciences, Harvard University, Cambridge, Massachusetts 02138, Institute for Advanced Research, Nagoya University, Nagoya 464-8601, Japan, and Aerodyne Research, Inc., Billerica, Massachusetts 08121

Oxidative processing (i.e., "aging") of organic aerosol particles in the troposphere affects their cloud condensation nuclei (CCN) activity, yet the chemical mechanisms remain poorly understood. In this study, oleic acid aerosol particles were reacted with ozone while particle chemical composition and CCN activity were simultaneously monitored. The CCN activated fraction at $0.66 \pm 0.06\%$ supersaturation was zero for 200 nm mobility diameter particles exposed to 565 to 8320 ppmv O_3 for less than 30 s. For greater exposure times, however, the particles became CCN active. The corresponding chemical change shown in the particle mass spectra was the oxidation of aldehyde groups to form carboxylic acid groups. Specifically, 9-oxononanoic acid was oxidized to azelaic acid, although the azelaic acid remained a minor component, comprising 3–5% of the mass in the CCN-inactive particles compared to 4–6% in the CCN-active particles. Similarly, the aldehyde groups of α-acyloxyalkylhydroperoxide (AAHP) products were also oxidized to carboxylic acid groups. On a mass basis, this conversion was at least as important as the increased azelaic acid yield. Analysis of our results with Köhler theory suggests that an increase in the water-soluble material brought about by the aldehyde-to-carboxylic acid conversion is an insufficient explanation for the increased CCN activity. An increased concentration of surface-active species, which decreases the surface tension of the aqueous droplet during activation, is an interpretation consistent with the chemical composition observations and Köhler theory. These results suggest that small changes in particle chemical composition caused by oxidation could increase the CCN activity of tropospheric aerosol particles during their atmospheric residence time.

1. Introduction

Organic aerosol particles in the atmosphere can be transformed from a hydrophobic to a hydrophilic state by several physical and chemical processes, which are collectively referred to as aging.[1,2] Hydrophilic particles have increased cloud condensation nuclei (CCN) activity compared to their hydrophobic counterparts. At present, many climate and atmospheric chemistry models include particle aging processes[3–5] as a simple conversion from a hydrophobic to a hydrophilic state after 1 to 2 days in the atmosphere.[2] The time scale of this conversion, however, is arguably not uniformly applicable to all aerosol particles on a global scale, as aging times should, in large part, vary locally with the concentrations of photochemically produced oxidants and condensates. Before a more accurate representation can be included in models, however, a more detailed understanding of the hydrophobic-to-hydrophilic aging mechanisms of organic aerosol particles, as well as consequent effects on CCN activity, is necessary.[2]

In one chemical aging mechanism, the condensed-phase molecules of the aerosol particles react heterogeneously with gas-phase atmospheric oxidants such as O_3, OH, and NO_3.[1] Heterogeneous chemistry is particularly important for the ozonolysis of unsaturated organic molecules because the rate constants for reaction of ozone with alkenes in the condensed phase[6–10] are typically 10^3 times faster than in the gas phase.[11] Thus, the condensed-phase ozonolysis of alkenes, in particular oleic acid, has been an area of intense research over the past few years.[6–10,12–25] In addition to chemical aging, physical aging can also occur in the atmosphere when soluble material, such as sulfate, nitrate, or secondary organic aerosol, collects on aerosol particles through condensation.[1,2,26,27] Cloud processing is also an important aging mechanism.[28–30]

The present paper reports on the results of oleic acid ozonolysis as a model system to investigate the role of heterogeneous oxidation in influencing the CCN properties of organic aerosol particles. The ozonolysis of oleic acid has served as a model system to investigate aerosol aging for several reasons.[25] Oleic acid is the most prevalent fatty acid in the cell walls of living organisms and is a major component in many cooking oils and lards.[31] As a result, it is found in ambient atmospheric aerosol particles and has been suggested as a marker for meat cooking.[32–34] Moreover, oleic acid has many chemical and physical properties that make it convenient for study in the laboratory: it is a liquid at room temperature, has a low vapor pressure, and is commercially available in high purity. Finally, a large body of literature now exists describing the kinetics, products, and mechanisms of the oleic acid ozonolysis reaction in aerosol particles.[6–10,12–25,35,36]

A simplified chemical mechanism of the ozonolysis of oleic acid is shown in Figure 1. Breakdown of the primary ozonide yields two excited-state Criegee intermediates (ECIs) and two

------

[†] School of Engineering and Applied Sciences, Harvard University.
[‡] Institute for Advanced Research, Nagoya University.
[§] Aerodyne Research, Inc.
* To whom correspondence should be addressed. E-mail: scot_martin@harvard.edu. Web page: www.deas.harvard.edu/environmental-chemistry.
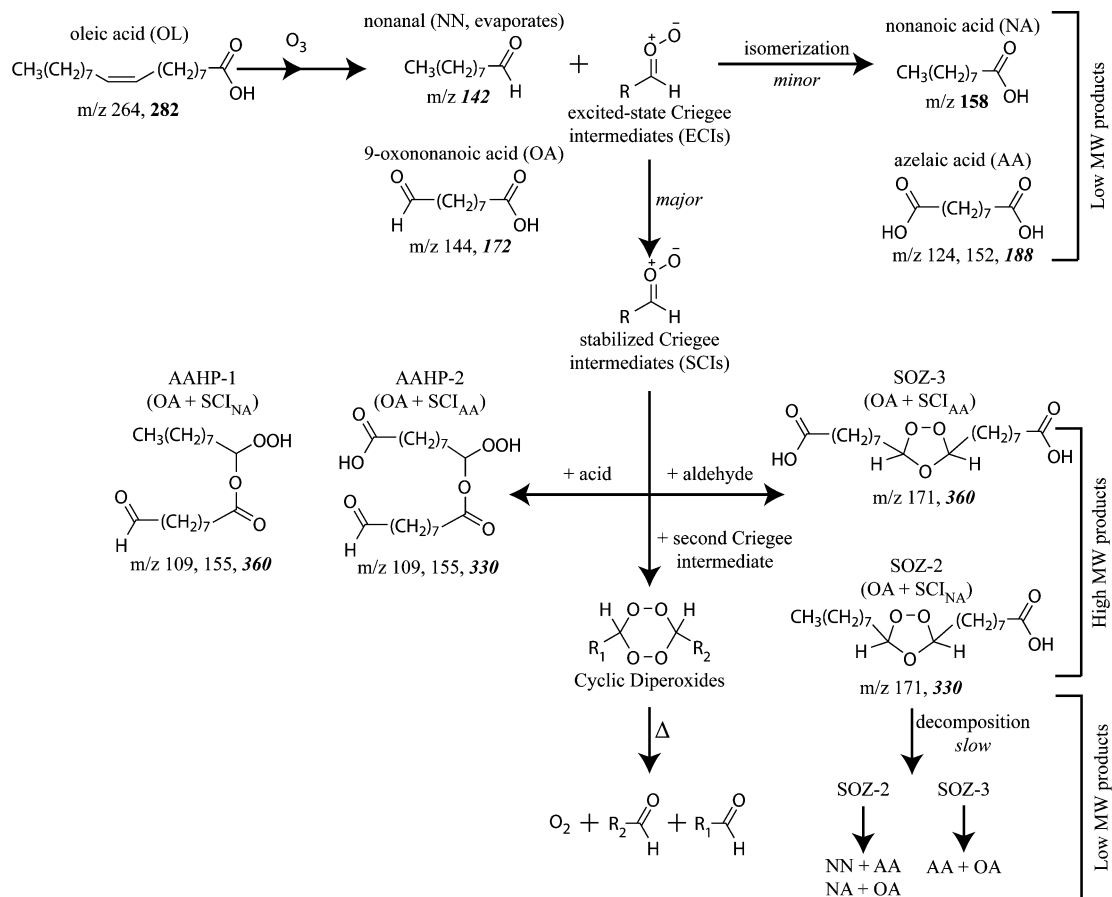
Aerosol CCN Properties

J. Phys. Chem. A, Vol. 111, No. 17, 2007 **3359**

Figure 1. Reaction pathways and products of the ozonolysis of oleic acid. For simplicity, reactions of stabilized Criegee intermediates with nonanoic acid and azelaic acid, which form with low yield, are not shown. Oligomerization reactions by the addition of Criegee intermediates to AAHPs and SOZs that bear aldehyde or acid functionalities are also omitted. The *m/z* values of the electron-impact fragment ions used to identify each species are given. Molecular weights are shown in bold and are italicized if the molecular ion is not observed in the mass spectra. AAHP and SOZ labeling follows that of Ziemann.[21]

stable products, nonanal and 9-oxononanoic acid. Nonanal, however, evaporates from the condensed phase.[7,10,17] As a major pathway, the ECIs vibrationally relax in the solvent, forming stabilized Criegee intermediates (SCIs), which subsequently react with other functional groups. As a minor pathway, the ECIs possibly isomerize to form nonanoic acid and azelaic acid in yields of 2−4%,[16,21] although these products arguably may instead form by the breakdown of some fraction of secondary ozonides.[37] Thus, the major monomeric product in the condensed phase is 9-oxononanoic acid, which has both aldehyde and carboxylic acid groups available for oligomerization reactions with the SCIs.

Oligomerization reactions are afforded by double moieties on 9-oxononanoic acid and azelaic acid.[35] Reactions of the two SCIs with the two functionalities of 9-oxononanoic acid produce the C_{18} α-acyloxyalkyl hydroperoxides (AAHPs) and secondary ozonides (SOZs) shown in Figure 1. The C_{18} compounds resulting from the reaction of the SCIs with azelaic acid, nonanoic acid, and unevaporated nonanal form in much smaller yields because of the low concentrations of the latter three species. C_{18} compounds can be indefinitely lengthened (i.e., C_{27}, C_{36}, etc.) so long as an aldehyde or carboxylic acid group remains.[19,21,22,35] Cyclic diperoxides are believed to form from the bimolecular reaction of two SCIs.[15,21] Their yield should be low in reaction media having high concentrations of carboxylic acid or aldehyde groups, which scavenge SCIs before they can react with another SCI.

Regarding the CCN activity of the products of oleic acid ozonolysis, Broekhuizen et al. showed that exposure to high ozone levels transforms oleic acid aerosol particles from CCN-inactive to CCN-active.[13] The transition occurs, however, only for an ozone exposure that is 10^3 times in excess of that required to completely consume the oleic acid.[16] To date, the chemical composition of ozonized oleic acid aerosol particles has been investigated only for ozone exposures well below those necessary for CCN activation.[6−8,10,12,14−23] The requirement of large excess ozone for CCN activation implies that, compared to Figure 1, new chemical products and/or reaction pathways must be responsible for activation. To this end, in the study described herein, oleic acid particles are subjected to increasing ozone exposure while CCN activity and chemical composition are simultaneously monitored. With this information, a detailed chemical mechanism is developed and discussed within the framework of Köhler theory to rationalize the increase in CCN activity.

2. Experimental Section

A schematic diagram of the experimental apparatus is shown in Figure 2. The apparatus consists of polydisperse aerosol generation by either atomization or homogeneous nucleation, diameter classification by a differential mobility analyzer (DMA) to obtain a monodisperse aerosol, chemical reaction between the aerosol particles and ozone in a flow tube (298 K, atmospheric pressure, and 0% relative humidity), and analysis by a quadrupole aerosol mass spectrometer (Q-AMS) and cloud condensation nucleus counter (CCNC).

2.1. Particle Generation and Classification. Oleic acid aerosol was generated by two methods, homogeneous nucleation
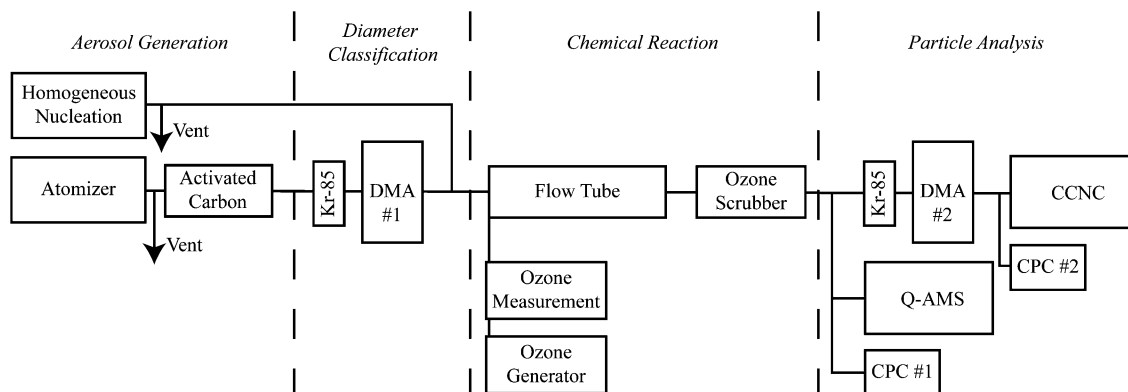
Figure 2. Schematic diagram of the experimental apparatus for the generation, classification, chemical reaction, and analysis of ozonized oleic acid aerosol particles. Key: Kr-85, [85]Kr bipolar charger; DMA, differential mobility analyzer; CPC, condensation particle counter; Q-AMS, quadrupole aerosol mass spectrometer; and CCNC, cloud condensation nucleus counter. (As necessary, DMA #2 and the CPC #2 are operated as a scanning mobility particle sizer (SMPS) to measure the particle number size distribution.)

and atomization. Aerosol generated by atomizing solutions (0.4 wt %) of oleic acid (99% purity, Aldrich) in methanol ($\geq$99.8%, EMD) or ethyl acetate ($\geq$99.8%, EMD) passed with 0.38 Lpm N_2 through a 0.8-m diffusion dryer (13 mm ID) filled with activated carbon to remove the solvent. The aerosol continued through a [85]Kr bipolar charger and a differential mobility analyzer (DMA #1; TSI, 3071, open sheath flow), which was used to select particles having a 200 nm geometric mean mobility diameter. Particle charge was assumed to have no effect on chemical reactivity. A 10:1 sheath-to-aerosol flow (N_2 carrier gas) was used in DMA #1, and the resulting particle size distribution had a geometric standard deviation of 1.08 (lognormal distribution). The integrated number concentration was $(0.5-5.0) \times 10^4$ particles cm^{-3}. The corresponding mass loading was $100-1000$ μg m^{-3}. In comparison, the vapor pressure of oleic acid (2.4 μg m^{-3} at 298 K)[38] is much lower, avoiding any artifact of particle size change inside DMA #1 as a result of evaporation due to the sheath flow dilution.[38,39]

Homogenously nucleated aerosol particles were produced by passing N_2 gas (UHP, 99.999%) over a few drops of oleic acid in a 100 mL round-bottom flask heated to $100-110$ °C. The aerosol was not passed through DMA #1. The particle size distribution had a geometric mean diameter of $250-300$ nm, a geometric standard deviation of $1.1-1.2$, a lognormal size distribution, and an integrated number concentration of $(0.5-5.0) \times 10^4$ particles cm^{-3}. The corresponding mass loading was $100-1000$ μg m^{-3}.

2.2. Chemical Reaction. The oleic acid aerosol particles were introduced at 0.38 Lpm through a movable injector into the center of a 120 cm long, 5.1 cm diameter laminar flow tube. The residence time of the particles in the flow tube was controlled from 5 to 50 s. In a separate diagnostic measurement, the particle residence time was measured by pulsing aerosol into the flow tube and recording the time between pulse initiation and detection. After appropriate corrections for the time required for the particles to travel through connecting tubing, the measured residence time was 90% of the expected value for laminar flow[40] and fewer than 5% of the particles were lost, even for the longest residence times studied.

A sheath flow containing ozone in 90% O_2 and 10% N_2 was introduced upstream of the particle injector at 1.07 Lpm into the flow tube. Ozone was produced at mixing ratios of $565-8320$ ppmv ($1.4 - 20.0$ g m^{-3}) by passing oxygen gas (UHP, 99.994%) through a variable corona discharge (Azco Industries Ltd., HTU-500G2). Therefore, the ozone concentration exceeded the oleic acid concentration by a factor of 10^3-10^5. Ozone mixing ratios were calculated from the measured absorbance

at 254 nm over a 1 cm path length using a cross section of 1.15 $\times 10^{-17}$ cm^2.[41] The sheath flow was regulated with an accuracy of 1% using mass flow controllers (MKS, 100B). The aerosol particles then passed through a diffusion tube having an outer annulus filled with ozone destruction catalyst (Carus Chemical, Carulite 200), which reduced the ozone mixing ratio by a factor of at least 10^3 (i.e., O_3 could no longer be detected by our methods).

At each injector position, the nominal ozone exposure was calculated as the product of the ozone concentration in the sheath flow (corrected for dilution) and the residence time of the particles in the flow tube. Two approximations in this calculation were that the ozone thoroughly and immediately mixed with the particles when the sheath and injector flows met and that the ozone was immediately removed from the gas phase upon contact with the ozone destruction catalyst.

2.3. Particle Analysis. Downstream of ozone removal, the aerosol flow was split three ways for particle analysis. The first part of the flow was isokinetically sampled by an Aerodyne Q-AMS.[42,43] The Q-AMS mass spectra provided information on the chemical composition of the particles. In addition, the Q-AMS measured the mass loading and the aerodynamic size distribution of the aerosol particles.

In brief, the Q-AMS functioned as follows.[42,43] Particles were focused by an aerodynamic lens[44,45] on to a cylindrical heater where the non-refractory components of the aerosol were flash vaporized. Molecules in the resultant vapor cloud were ionized at 70 eV by electron impact and analyzed with a quadrupole mass filter (Balzers, QMA 430). One difference in the operation of the Q-AMS for this study compared to its normal operation was that a lower heater temperature was employed (i.e., 250 °C compared to $500-600$ °C). The lower heater temperature was sufficient to volatilize the organic mass while somewhat reducing the thermal fragmentation of the organic molecules and, therefore, affording more information-rich mass spectra.

The second part of the split flow entered a condensation particle counter (CPC #1; TSI, 3022A) for measurement of the total particle number concentration. The third part of the split flow passed through a [85]Kr bipolar charger and a DMA (DMA #2; TSI, 3800, recirculating sheath flow) to obtain a flow of monodisperse aerosol particles. Mobility diameters of 200 and 181 nm were selected for homogeneously nucleated and atomized particles, respectively. In the case of the atomized particles, the 200 nm monodisperse mode selected by DMA #1 (cf. section 2.1) decreased to a 181 nm mode following ozonolysis.[13,17] In the case of homogeneous nucleation, a polydisperse aerosol sample was employed, so analysis of 200

Aerosol CCN Properties

J. Phys. Chem. A, Vol. 111, No. 17, 2007 **3361**

nm particles was possible. Although the particles were already charged after exiting DMA #1, the additional bipolar charger in conjunction with DMA #2 greatly reduced the relative concentration of doubly charged particles in the aerosol flow. The aerosol exiting DMA #2 was sampled in parallel by a CCNC (Droplet Measurement Technologies)[46,47] and CPC #2 (TSI, 3782). The activated fraction (F_a), calculated as the ratio of the number of particles counted by the CCNC to the number of particles detected by CPC #2, quantified the propensity of a population of aerosol particles to form cloud droplets. The CCNC was set to a nominal supersaturation of 0.6%, corresponding to a calibrated supersaturation of $0.66 \pm 0.06\%$.

2.4. CCNC Calibration. The CCNC instrument[46,47] regulated a temperature gradient within a wetted wall flow tube. Pointedly, supersaturation was not directly measured and calibration with test aerosols was necessary. We used monodisperse NaCl and $(NH_4)_2SO_4$ test aerosols for the calibration at 0.3 and 1.0% supersaturation. A full description of the calibration is given in Appendix 1. The results showed that the actual supersaturation was between 0.60 and 0.72% when the instrument was adjusted to the manufacturer's nominal setting of 0.6% supersaturation.

3. Results and Discussion

3.1. Control Experiments. Control experiments were conducted to validate our experimental method through comparison with literature data and to provide a baseline for the CCN activation experiments. No CCN activity at $0.66 \pm 0.06\%$ supersaturation was observed for unreacted oleic acid aerosol particles as large as 350 nm, both for generation by homogeneous nucleation and by atomization in ethyl acetate. Reacted oleic acid particles at 200 nm mobility diameter remained CCN-inactive for ozone exposures up to 0.01 atm s, even though the oleic acid in the particles had been completely consumed by ozone and the products included a high abundance of oxygenated organic molecules. These results agree well with the observations of Broekhuizen et al.,[13] who found that oleic acid particles remained CCN-inactive at 0.6% supersaturation for ozone exposures less than 0.01 atm s and for dry diameters of up to 300 nm.[13]

In a separate experiment oriented toward a comparison of our results with those of Broekhuizen et al.,[13] we scanned particle diameter while holding supersaturation at $0.66 \pm 0.06\%$ and ozone exposure at 0.1 atm s. The reacted particles activated at 160 nm. Broekhuizen et al. reported an activation diameter of 161 nm at 0.6% supersaturation and 0.42 atm s.[13] We consider our results and those of Broekhuizen et al.[13] in agreement, within experimental uncertainty.

3.2. CCN Activation. The activated fractions of reacted oleic acid aerosol particles are shown in Figure 3 for increasing ozone exposure. For a particular ozone mixing ratio, the exposure was varied by increasing the ozonolysis time. As seen in Figure 3, the oleic acid particles were transformed from CCN-inactive to CCN-active by increasing exposure to ozone. The exposures required to activate 181 nm particles atomized from ethyl acetate (Figure 3A) were slightly lower than those required to activate 200 nm particles generated by homogeneous nucleation (Figure 3B). The explanation may be that a small amount of ethyl acetate, which has a water solubility of 64 g L^{-1},[48] remained in the atomized particles, thereby enhancing CCN activity (cf. Appendix 2). Data corresponding to particles generated by atomization are therefore excluded from most of the further analysis of this study.

3.3. The "atm s" Reaction Coordinate. A common treatment in literature is to combine the concentration of an excess
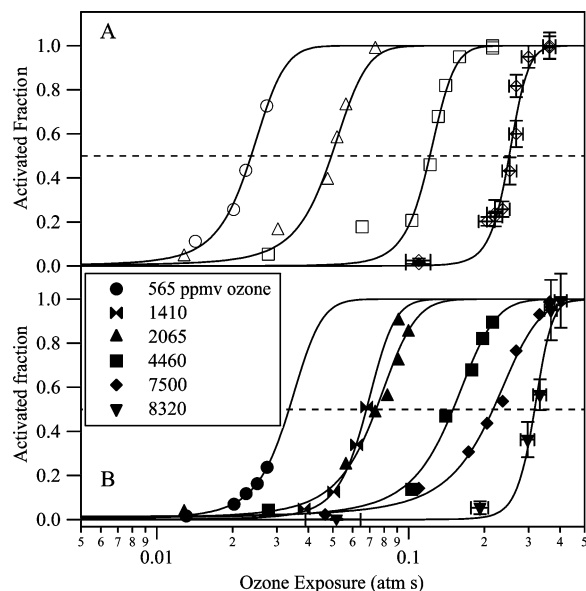

Figure 3. CCN activated fraction at $0.66 \pm 0.06\%$ supersaturation for 181 nm mobility diameter particles generated by atomization and ozonolysis (panel A) and for 200 nm mobility diameter particles generated by homogeneous nucleation and ozonolysis (panel B) as a function of ozone exposure (298 K, atmospheric pressure, and 0% RH). A sigmoidal fit is applied to each data set. The dashed line indicates an activated fraction of 0.5. Along the abscissa, error bars represent combined uncertainties in the ozone mixing ratio, the sheath and aerosol flow rates, and the ozone/particle interaction time. Along the ordinate, error bars represent combined uncertainties in the counting efficiencies of the CCNC and the CPC. Error bars are shown only for the highest ozone exposure but are similar at lower exposures.

reagent (e.g., O_3) and the reaction time into a single unit termed "exposure" when describing pseudo-first-order kinetics because exposure can sometimes serve as a composite variable that accurately describes the extent of reaction.[6,8,9,13,16,20,49] Figure 3, however, shows that the CCN-activation curves do not converge when plotted on an exposure axis. Instead, substantially higher ozone exposures are required to achieve activation as the ozone mixing ratio was increased. The implication is that the activation of oleic acid by intense ozonolysis does not appear to follow a pseudo-first-order rate law, suggesting that ozone concentration and exposure time do not have equal weighting in determining the CCN activity of the aged particles.

Figure 4 better illustrates this phenomenon. The exposure time required to reach an activated fraction of 0.5 is plotted for several ozone mixing ratios. Above 1000 ppmv O_3, activation appears to depend only on reaction time (i.e., approximately 30 s regardless of ozone concentration). The implication could be a surface saturation effect at these high ozone concentrations. For lower ozone concentrations (e.g., 500 ppmv in Figure 4), there is sensitivity to the reaction time.

3.4. Changes to Mass Spectra: Observations. Figure 5 shows mass spectra obtained for oleic acid aerosol particles prior to and after ozonolysis. The spectra in Figure 5, panels A and B, agree well with those reported in the literature for oleic acid and its ozonolysis products.[6,16,21] We are aware of no previous mass spectra published for oleic acid aerosol particles having ozone exposures as high as those corresponding to Figure 5C. Comparison of panels B and C of Figure 5 to panel A shows that oleic acid reacts to completion (i.e., the absence of peaks at m/z 264 and 282 in parts B and C), even for the lowest ozone exposure studied (Figure 5B).

The mass spectra of reacted but CCN-inactive particles (Figure 5B) and reacted, CCN-active particles (Figure 5C) are
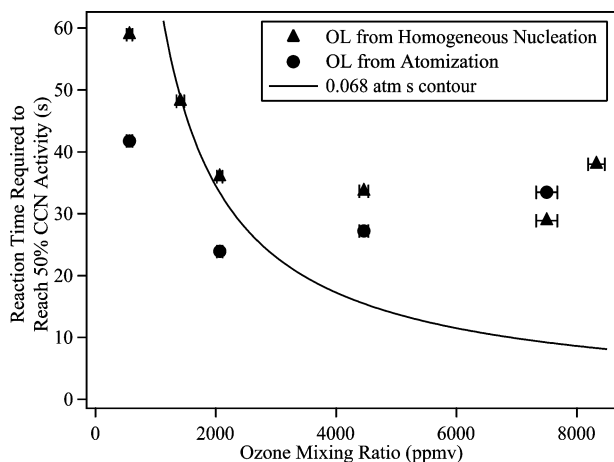
3362 *J. Phys. Chem. A, Vol. 111, No. 17, 2007*

Shilling et al.

Figure 4. Reaction times required to reach 50% CCN activity for several ozone concentrations, as derived from the data shown in Figure 3. A representative contour of constant exposure (0.068 atm s) is also shown.
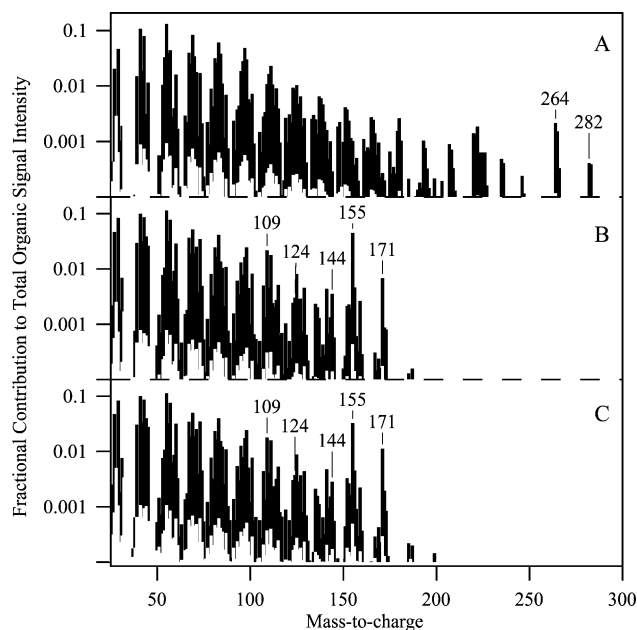

Figure 5. Mass spectra of oleic acid aerosol particles before exposure to ozone (panel A), after 0.0036 atm s of ozone exposure (panel B), and after 0.402 atm s of ozone exposure (panel C). The corresponding CCN activated fractions are 0.0 for panels A and B but 0.993 for panel C. Spectra are normalized to the total organic signal intensity. White bars indicate the uncertainty (3σ) associated with the signal intensity at each m/z value. Important marker peaks are indicated. Conditions: particles generated by homogeneous nucleation and reacted at 298 K, atmospheric pressure, and 0% RH.

similar, indicating that the differences in the chemical compositions of inactive and active particles are small. Small changes, however, can be highlighted by a fractional difference plot between groups of averaged spectra (Figure 6). Fractional difference ($\Delta_{m/z}$) is given by $\Delta_{m/z} = (I^A_{m/z} - I^B_{m/z})/I^B_{m/z}$, where $I^A_{m/z}$ and $I^B_{m/z}$ are the signal intensities of the averaged spectra for a specific m/z value.[50] Mass spectra corresponding to the points in Figure 3B having $F_a > 0.9$ (i.e., CCN-active) were averaged and taken as group A, while mass spectra having $F_a < 0.1$ (i.e., CCN-inactive) were placed in group B. The spectrum in Figure 5B was, therefore, included in group B and that of Figure 5C in group A. Moreover, only m/z values having signal-to-noise ratios greater than 40 were included in the analysis. Spectra within group A were indistinguishable from one another, at least
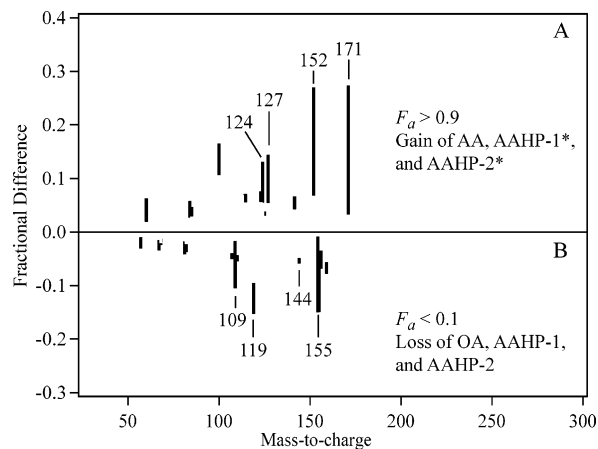

Figure 6. Fractional difference ($\Delta_{m/z}$) calculated as: $\Delta_{m/z} = (I^A_{m/z} - I^B_{m/z})/I^B_{m/z}$, where $I^A_{m/z}$ and $I^B_{m/z}$ are the signal intensities of the averaged mass spectra for $F_a > 0.9$ and $F_a < 0.1$, respectively, for the data of Figure 3B. Signals having signal-to-noise ratios less than 40 are excluded from the analysis. Error bars (3σ) are shown as white bar overlays so that only statistically significant $\Delta_{m/z}$ values can be seen. Signals for Δ_{151} and Δ_{172} are removed from Figure 6 because, based on shoulders apparent in the raw data (not shown), they are artifacts of the strong signals at Δ_{152} and Δ_{171}. The full set of raw data corresponding to Figure 6 is included in the on-line Supporting Information as Table S1.

by our analysis methods, and this condition of intra-group similarity also held for group B.

In Figure 6, the heights of the black bars show the fractional difference at m/z values for which the fractional difference exceeded the signal-to-noise uncertainty. The height of a black bar represents the magnitude of the difference signal. The ratio of the difference signal compared to the uncertainty corresponds to the upper value of the black bar divided by the lower value. The absence of a black bar at a given m/z value either indicates that the uncertainty in the difference signal is greater than the difference signal itself or that the difference signal does not pass the signal-to-noise threshold criterion, signifying in both cases that there was not a statistically robust difference between the compared spectra at that m/z value.

3.5. Changes in Mass Spectra: Interpretation as Changes in Chemical Composition. As a result of both the extensive fragmentation caused by electron-impact ionization and the thermal decomposition of molecules on the Q-AMS heater, most of the signal intensity occurred below m/z 100, and molecular ion peaks were weak or unobserved. Therefore, m/z values of fragment ions were employed as tracers of the parent species. Assignment of m/z values to fragment ions and parent species is presented in Appendix 3. Fragmentation of the assigned parent species produced the majority of the spectral intensity at the indicated m/z tracer values (cf. Appendix 3), although other parent species made minor contributions to those signal intensities, too.

Figure 6 shows that, when the particles became CCN-active, the signal intensities having contributions from azelaic acid (m/z 124, +13.1% ± 5.4; m/z 152, +27.0% ± 6.8) and from AAHP-1* and AAHP-2* (m/z 127, +14.1% ± 5.4; m/z 171, +27.4% ± 3.2) increased while those having contributions from 9-oxononanoic acid (m/z 144, −5.9% ± 4.8) and from AAHP-1 and AAHP-2 (m/z 109, −13.1% ± 5.4; m/z 119, −15.3% ± 9.5; 155, −15.0% ± 1.1) decreased, where the percentage change and the associated uncertainty (3σ) for each marker signal are given in parentheses. Therefore, an increase in carboxylic acid functionalities (i.e., gain of AA, AAHP-1*, and AAHP-2*) and
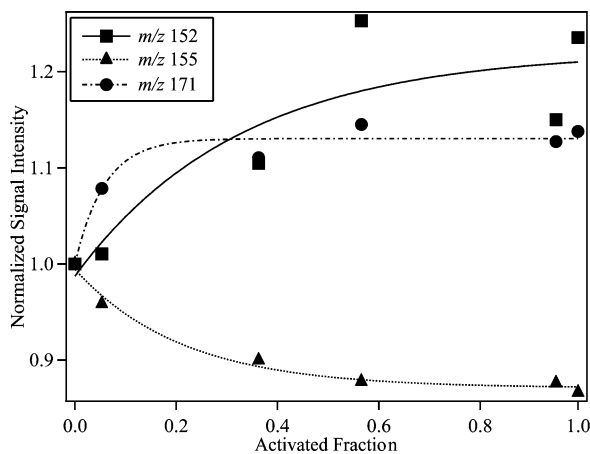
Figure 7. Signal intensities at m/z 152, m/z 155, and m/z 171 for increasing CCN activated fraction. Signal intensities are normalized to their values at $F_a = 0$. Lines shown are to guide the eye. Conditions: 8320 ppmv O_3 and 0.66 ± 0.06% supersaturation (cf. Figure 3B).

a decrease in aldehyde functionalities (i.e., loss of OA, AAHP-1, and AAHP-2) were associated with the increase in CCN activity. The structures of AAHP-1* and AAHP-2* are shown in Figure 8.

The association between CCN activity and the signal strengths of AA (m/z 152), AAHP-1* and AAHP-2* (m/z 171), and AAHP-1 and AAHP-2 (m/z 155) is explicitly shown in Figure 7. Not shown is that the signal intensities did not vary between the lower ozone exposures required to eliminate oleic acid and the higher ozone exposures for which the CCN activated fraction was still zero. At a critical point, however, further increases in ozone exposure resulted in increases in CCN activity (cf. Figure 3). In conjunction, the signal intensities at m/z 152/171 smoothly increased while the signal intensity at m/z 155 smoothly decreased, in agreement with the analysis presented for Figure 6.

The conversion of aldehydes to carboxylic acids is a slow but known reaction for high ozone exposure.[51,52] Ozone reacts in the condensed phase approximately 10^3 times slower with aldehydes than with alkenes,[37,51] which is in approximate agreement with the observation that the ozone exposure required to eliminate oleic acid was 1000-fold smaller than that necessary for CCN activation. The mechanism for aldehyde ozonolysis is shown in Figure 8.[53,54] A two-step evolution therefore leads to CCN activation. The products shown in Figure 1 form in step 1, but, upon further exposure, some of the aldehydes begin to react with ozone. An alternate hypothesis that the chemical pathways of step 1 change is ruled out because increased reaction time changed neither the activated fraction nor the mass spectrum until a critical reaction time was reached. The concept of the two-step chemical evolution is represented by the pie charts in Figure 9.

By calibrating the Q-AMS with commercially available azelaic acid and 9-oxononanoic acid, we determined the mass percent contribution of these molecules in both the CCN-inactive and CCN-active aerosol particles.[16] Azelaic acid increased from 3−5% to 4−6% by mass upon activation. The corresponding 6% loss of 9-oxononanoic acid relative to a base yield of 30% by mass[16,21] was consistent with the increase in AA, suggesting stoichiometric conversion of OA to AA. Because authentic standards of the AAHP and SOZ compounds were not available, we were unable to perform an analogous analysis for the signals at m/z 109 and 155 (AAHP-1 and AAHP-2) and 127 and 171 (AAHP-1* and AAHP-2*). Nevertheless, because AAHP-1 and

AAHP-2 both contain 9-oxononanoic acid as a monomer unit (Figure 1), we believe that the conversions of AAHP-1 to AAHP-1* and AAHP-2 to AAHP-2* were at least as important on a mass basis as the conversion of OA to AA.

Signal intensities at m/z 43 and 44 are widely employed in the AMS literature as indicators of the extent of organic particle oxidation,[50,55−57] so an expectation could be that an aldehyde-to-acid conversion would be apparent as relative changes in these peak intensities. Neither an increase in the signal intensity at m/z 44, which is a common fragment oxo- and dicarboxylic acids (CO_2^+),[57] nor a decrease at m/z 43, which is a fragment of oxidized organic molecules containing carbonyl groups ($C_2H_3O^+$) and also of alkanes ($C_3H_7^+$),[57] was detected, presumably because the magnitude of the change was small relative to the noise. The signal intensities at m/z 43 and 44 were intense in all spectra (Figure 5), and the number of aldehyde functionalities converted to carboxylic acid functionalities was small relative to the total set of functional groups contributing to the signal intensities at m/z 43 and 44.

Recent literature reports support the formation of oligomers of C_{27} and greater in ozonized oleic acid samples.[19,22,35] Direct detection of these oligomers in the Q-AMS, however, is not possible because their molecular ions, even if formed, would have m/z values beyond the upper limit of the scanning range of the Q-AMS, namely m/z 390. Indirect detection of the oligomers is complicated by non-unique fragment ions: C_{27} and larger oligomers are expected to form fragment ions identical to those of the C_{18} oligomers and the C_9 monomer units. Contribution of larger oligomers to the signal intensities of maker peaks may help to rationalize the nonuniform changes in the signal intensities of the marker peaks of a particular species upon particle activation (e.g., the intensity at m/z 124 changes by +13.1% ± 5.4 compared to +27.0% ± 6.8 at m/z 152, both of which are markers of AA).

3.6. Mechanism of CCN Activation. The results clearly show that a conversion of aldehydes to carboxylic acids by ozonolysis is associated with increasing CCN activity. In this section, we consider why these chemical changes lead to increasing CCN activity. A first hypothesis is that ozonolysis increases the amount of water-soluble material in the particles, which facilitates activation. A second hypothesis is that ozonolysis produces surface-active species that reduce surface tension and thereby facilitate activation.

We can show, using our data set, that the first hypothesis is not chemically tenable, as follows. Köhler theory can model the activation of a particle composed of more-soluble and less-soluble organic molecules.[58] The base case parameters of our experimental conditions are a dry diameter of 200 nm, a density of water (1.0 g cm^{-3}), and a surface tension of water (0.072 N m^{-1}). Although the ozonized particle is a complex mixture of many components, azelaic acid (solubility of 0.0024 kg/kg solution)[59] is the most soluble product, and, as a limiting case, we select it to represent the more-soluble organic molecules. To represent the less-soluble organic molecules, we use the properties of stearic acid (solubility of 2.9 × 10^{-6} kg/kg solution)[60] to approximate the solubility of oleic acid. Figure 10 shows the modeling results for the base case as well as several sensitivity tests. A critical supersaturation of 1.05% is predicted for the activation of 200 nm particles containing 5% azelaic acid and 95% oleic acid (by volume, red line). This critical supersaturation is only slightly lower than that of pure oleic acid (1.07%, dark blue line). As a limit of high-end solubility, pure azelaic acid particles are modeled to activate at
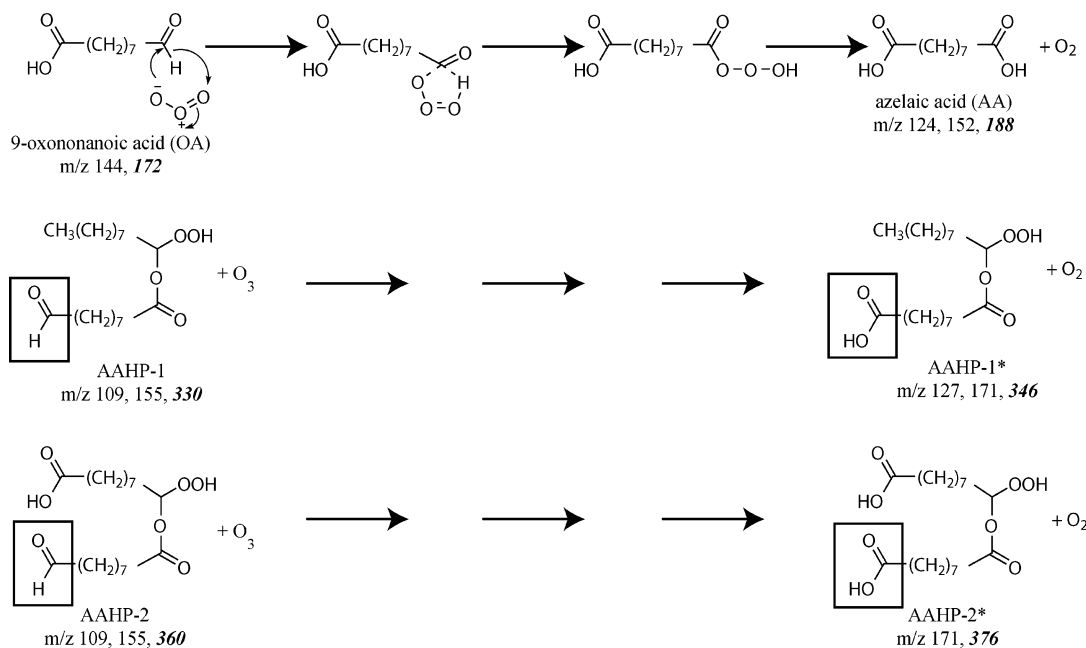
Figure 8. Chemical mechanism showing the oxidation of aldehydes to carboxylic acids by ozone.[51-54] The conversion of aldehyde to acid functionalities is associated with the increase in CCN activity observed for oleic acid aerosol particles at high ozone exposures. The meaning of the shown *m/z* values is the same as in Figure 1.
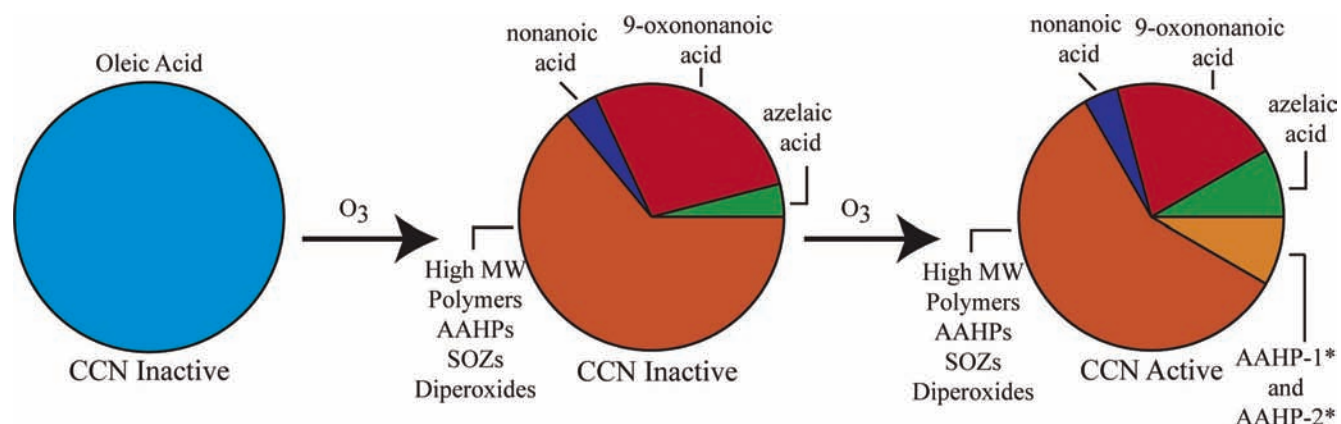

Figure 9. Representation of the chemical changes that occur upon activation of ozonized oleic acid aerosol particles. Aldehyde groups are oxidized to carboxylic acid groups, transforming AAHP-1, AAHP-2, and OA into AAHP-1*, AAHP-2*, and AA, respectively. The relative concentrations represented in the pie charts are approximate.

1.05% supersaturation (not shown), assuming the surface tension of pure water. These modeling results, therefore, indicate that an increased content of more-soluble material cannot alone explain the experimentally observed activation at 0.66 ± 0.06% supersaturation.

Although the production of soluble species has a minor effect on the modeled critical supersaturations (viz. comparison of the light blue and orange lines, Figure 10), the lowering of the solution surface tension through the production of surfactants has a significant effect (viz. comparison of the red and orange lines Figure 10). A surface tension of 0.042−0.048 N m⁻¹ (black and green lines, respectively, of Figure 10) leads to activation for the experimental conditions of 0.66 ± 0.06% supersaturation (gray area). In comparison, the surface tensions of saturated aqueous solutions of azelaic acid (0.061 N m⁻¹) and nonanoic acid (0.030 N m⁻¹), which are products of oleic acid ozonolysis, straddle this range.[59] Nonanoic acid does not appear to drive activation because its particle-phase concentration does not change as ozone exposure increases. We believe that molecules such as AAHP-1*, which is present in large quantities only in the CCN-active particles, lower the surface tension of the

activating droplets. AAHP-1* has a hydrophobic tail and a hydrophilic head, which are typical characteristics of surfactants. Moreover, the yield of AAHP-1 from the original oleic acid may be substantial (e.g., 10−15% on a carbon basis)[49] given that SCI_{NA} is a terminating group of oligomerization[35] and assuming that the yields of AAHPs exceed those of SOZs and diperoxides pathways in the carboxylic acid-rich reaction medium.[8,37,49] The second hypothesis of decreased surface tension accompanying the conversion of aldehydes to carboxylic acids is, therefore, a chemically reasonable explanation of the observations.

4. Conclusions and Atmospheric Implications

The results of this work show that the oxidative processing (i.e., "chemical aging") of aerosol particles can affect their CCN activity. A mechanism based upon surface tension lowering is presented for the ozonolysis of oleic acid particles. A qualitative summary of the chemical changes is shown in Figure 9. Oleic acid, shown in the left panel, reacts in step 1 to yield a mixture, shown in the center panel, of low-molecular-weight primary products and high-molecular-weight oligomers.
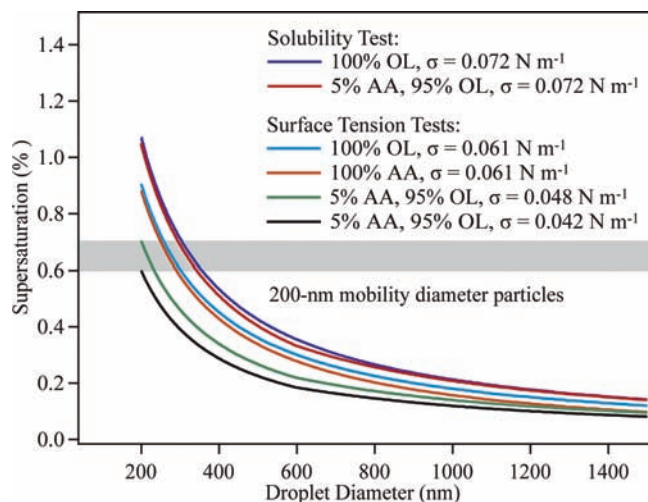
Aerosol CCN Properties

J. Phys. Chem. A, Vol. 111, No. 17, 2007 **3365**

Figure 10. Köhler curves for the activation of 200 nm organic particles composed of 100% OL with the surface tension of water (dark blue trace), 5% AA/95% OL with the surface tension of water (red trace), 100% OL with the surface tension of saturated aqueous AA (light blue trace), 100% AA with the surface tension of saturated aqueous AA (orange trace), 5% AA/95% OL with a surface tension of 0.048 N m^{-1} (green trace), and 5% AA/95% OL with a surface tension of 0.042 N m^{-1} (black trace). The gray range shows the supersaturation of the experimental measurements (i.e., 0.66 ± 0.06%). The AA and OL concentrations in the activating particles are limited by their aqueous solubilities (2.4×10^{-3} and 2.9×10^{-6} kg/kg solution, respectively).[59] Droplets are assumed to have the density of pure water at activation. Negligible interactions between aqueous AA and OL are assumed.

This mixture, although it contains a high abundance of oxygenated organic molecules, nevertheless remains CCN-inactive up to ozone exposures of 0.01 atm s, which is more than one hundred times the exposure required to completely consume the oleic acid. Upon further ozone exposure, in step 2, aldehyde groups on 9-oxononanoic acid, AAHP-1, and AAHP-2 react directly with ozone to form carboxylic acids (right panel). Our analysis concludes that this conversion of aldehydes to acids dramatically enhances the CCN activity of the particles because surface-active molecules such as AAHP-1* are formed.

These laboratory findings begin to provide a mechanistic and quantitative basis for further thinking on oxidative chemical aging reactions active in the troposphere, and two main implications are apparent. (1) Organic compounds bearing aldehyde functionalities occur in diverse populations of atmospheric aerosol particles.[27,61,62] Aldehyde-to-carboxylic acid conversion by ozonolysis may therefore be a chemical aging mechanism having widespread applicability. (2) Only small changes in chemical composition are necessary to alter the aerosol CCN properties. For example, approximately 6% of the 9-oxononanoic acid by mass was converted to azelaic acid upon activation. A similar mass-based conversion of AAHP-1 and AAHP-2 to AAHP-1* and AAHP-2* also occurred. Thus, the slow conversion of aldehydes to carboxylic acids over the lifetime of atmospheric particles may plausibly transform them from CCN-inactive to CCN-active, especially in the case that surface-active products form. In addition to the chemical aging mechanisms explored in this study, physical aging also occurs in the atmosphere when soluble material, such as sulfate, nitrate, or secondary organic aerosol, collects on the particles by coagulation or condensation. Further laboratory studies of both physical and chemical aging are well warranted.
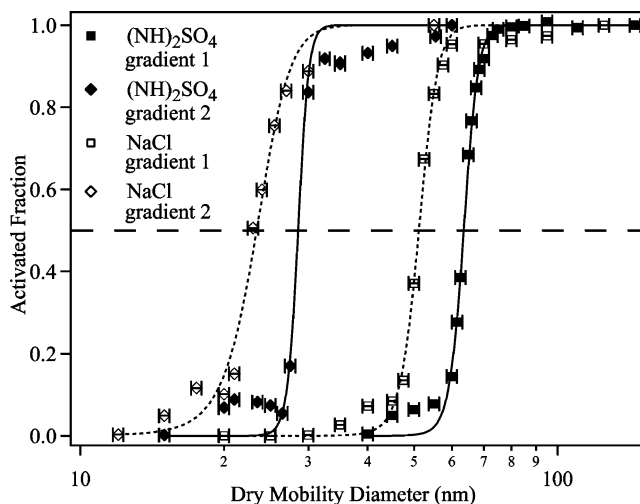
Figure A1. CCN activated fraction (F_a) for increasing dry mobility diameter of ammonium sulfate and sodium chloride calibration aerosols. Data are shown for instrument temperature gradients 1 (6.3 K) and 2 (17.8 K). The intersection of a sigmoidal fit to a data set with the dashed line at $F_a = 0.5$ corresponds to a CCN−activation mobility diameter given in Table 1. Nonzero activated fractions at diameters significantly smaller than the diameters of $F_a = 0.5$ correspond to multiply charged particles exiting DMA #2. Data are normalized to $F_a = 1.0$ at large diameter.

Appendix 1. CCNC Calibration

The calibration of the DMT CCNC instrument[46,47] was carried out by associating applied temperature gradients with the observed activation of calibration salts and their respective theoretical supersaturations. An atomizer (TSI, 3076) was used to generate an aerosol flow of either NaCl or $(NH_4)_2SO_4$ particles in nitrogen. This flow was diluted 10-fold, effloresced at less than 5% relative humidity in a diffusion dryer, passed through a ^{85}Kr bipolar charger, and size selected using a DMA (TSI, 3081). The aerosol flow was 0.8 Lpm, and the aerosol-to-sheath flow ratio was 1:10. The flow of monodisperse particles (100−1000 cm^{-3}, 1.06 geometric standard deviation) was split for sampling by a CPC (TSI, 3025) and the CCNC.

Inside the CCNC, the particles passed through a wetted, vertical, cylindrical column, in which a well-defined supersaturation was established by a temperature gradient along the centerline of the column.[46,47] Aerosol was sampled into the CCNC at 0.05 Lpm and the total flow through the column was 0.5 Lpm. An optical particle counter positioned at the outlet of the column detected and classified the particles into optical-diameter bins ranging from 0.75 to 10 μm. Particles having optical diameters larger than 1 μm were considered activated.

The activated fraction (F_a) was calculated as the number concentration of activated droplets counted by the CCNC divided by the total number concentration counted by the CPC. The activation diameter, defined as the dry diameter for an activated fraction of 0.50, was measured for increasing dry mobility diameter (Figure A1) and is given in Table 1 for each calibration condition.

The temperature-gradient-to-supersaturation calibration was obtained by use of eqs A1−A5 (vida infra) to associate the

3366 *J. Phys. Chem. A, Vol. 111, No. 17, 2007*

Shilling et al.

TABLE 1: CCN-Activation Mobility Diameters (Based on the Inflection Point of the Sigmoidal Fits Shown in Figure 11) of Ammonium Sulfate and Sodium Chloride Calibration Aerosols[a]

	activation diameter	
	gradient 1	gradient 2
$(NH_4)_2SO_4$	63.5 ± 1.6 nm (68 ± 8)	28.6 ± 0.7 nm (30 ± 3)
NaCl	50.9 ± 1.2 nm (51 ± 3)	23.0 ± 0.6 nm (23 ± 1)

[a] Uncertainties are based on the absolute accuracy of the classifier performance.[67] The values in parentheses are the ranges of activation diameters reported in the literature[69] assuming that the applied temperature gradients 1 (6.3 K) and 2 (17.8 K) in the CCN instrument correspond to 0.3% and 1.0% supersaturations, respectively (i.e., manufacturer's calibration).

activation diameters given in Table 1 with critical supersaturations. The Köhler model of Brechtel and Kreidenweis for aqueous droplets,[63] incorporating a form of the Pitzer osmotic coefficient[64] for water activity, was employed as follows:

$$s = 100\left(a_w \exp\left(\frac{4\sigma M_w}{RT\rho_w D_{aq}}\right) - 1\right) \qquad (A1)$$

where s (%) is the supersaturation relative to a plane of liquid water, a_w is the water activity of the solution, σ is the solution-vapor surface tension, M_w is the molecular weight of pure water, R is the universal gas constant, T is the solution temperature, ρ_w is the density of pure water, and D_{aq} is the aqueous particle diameter. The critical supersaturation s_c of activation is the value of s for which the condition $\partial s/\partial D_{aq} = 0$ is satisfied.

The Raoult term in eq A1 is calculated as follows:

$$a_w = \exp(-M_w \nu \Phi m) \qquad (A2)$$

where ν is the number of ions from the dissociation of one solute molecule (i.e., $\nu = 2$ for NaCl and $\nu = 3$ for $(NH_4)_2SO_4$), Φ is the osmotic coefficient, and m is the solution molality. For the osmotic coefficient, we employ:

$$\Phi = 1 - \frac{A\sqrt{Y_a c}}{\sqrt{2} + b_{pit}\sqrt{Y_b c}} + 2Y_c c \beta_0 \qquad (A3)$$

where $c = 1000 m M_w/\rho_s$ and A, b_{pit}, Y_a, Y_b, Y_c, and β_0 are parameters as given by Brechtel and Kreidenweis.[63]

The Kelvin term in eq A1 depends on the aqueous particle diameter, which is related to the volume-equivalent dry diameter $D_{ve,dry}$ by the dry particle density ρ_s, the weight fraction w_t of the salt solute in the solution, and the density of the aqueous particle ρ_{aq}, as follows:[65]

$$D_{aq} = \left(\frac{\rho_s}{w_t \rho_{aq}}\right)^{1/3} D_{ve,dry} \qquad (A4)$$

for which $w_t = m M_s/(1 + m M_s)$, where M_s is the molecular weight of the solute.

The volume-equivalent dry diameter is related to the dry mobility diameter ($D_{m,dry}$) (i.e., the size classified by the DMA) by a shape factor (χ) for non-spherical particles:

$$\chi C_c(D_{m,dry}) D_{ve,dry} = C_c(D_{ve,dry}) D_{m,dry} \qquad (A5)$$

where C_c is the Cunningham slip correction. The shapes of salt particles depend on their method of preparation and the subsequent relative humidity history, among other factors.[39] Ammonium sulfate particles prepared by our method of atomi-

TABLE 2: Supersaturations Calculated from the Activation Mobility Diameters Given in Table 1 and Equations A1 to A5[a]

	effective supersaturation	
	gradient 1	gradient 2
$(NH_4)_2SO_4$, $\Phi = 1$, $\chi = 1.00$	0.271 to 0.292%	0.898 to 0.966%
$(NH_4)_2SO_4$, $\chi = 1.00$	0.299 to 0.323%	1.05 to 1.14%
*$(NH_4)_2SO_4$, $\chi = 1.02$	0.308 to 0.334%	1.09 to 1.18%
*NaCl	0.336 to 0.361%	1.12 to 1.21%
manufacturer's calibration ($(NH_4)_2SO_4$, $\Phi = 1$, $\chi = 1.00$)	0.30%	1.00%

[a] The supersaturation range corresponds to the upper and lower limits of particle diameters given in Table 1. Results are also shown assuming spherical ($\chi = 1.0$) and slightly nonspherical ($\chi = 1.02$) ammonium sulfate particles.[39] The entries we recommend are marked by asterisks.

zation and subsequent efflorescence are slightly nonspherical when prepared ($\chi = 1.02$).[39] We therefore employ $\chi = 1.02$ for our calibration, although we also include a comparison to $\chi = 1.00$ because this value is widely assumed in the literature. Sodium chloride particles prepared by our method are cubic, having a shape factor of 1.08 at low Knudsen number (Kn) and 1.24 at high Kn.[66] For a DMA operated at 1 atm, the condition holds that $0.1 < Kn < 10$, and in this case the intermediate shape factor is calculated by interpolation.[66] For mobility diameters of 23 and 51 nm, as given in Table 1 for cubic NaCl particles, the corresponding χ values are 1.23 and 1.18, respectively.

Equations A1 to A5 together define $s_c(D_{m,dry})$. For the calibration, the activation diameters of Table 1 therefore indicate the supersaturation inside the CCNC. Results are shown in Table 2. For comparison, the settings of the CCNC manufacturer included in the instrument's software at these same temperature gradients correspond to 0.30% and 1% supersaturation. Although the manufacturer carried out a similar calibration as ours, the analysis differed in that only $(NH_4)_2SO_4$ particles were studied and $\Phi = 1$ and $\chi = 1$ were assumed in eqs A2 and A5, respectively. The uncertainty of the calibration stems in our analysis from the uncertainty associated with the activation diameter and, hence, ultimately with classifier performance.[67] The conclusion from the results shown in Table 2 is that a laboratory recalibration of the instrument after delivery from the manufacturer is recommended.

Appendix 2. CCN Activity of Oleic Acid Atomized from Methanol

An activated fraction of 0.5 was observed at a mobility diameter of 195 nm for unreacted oleic acid aerosol particles generated from the atomization of methanol solutions. CCN activity in this case, considering the absence of CCN activity for oleic acid particles generated by homogeneous nucleation or atomization from ethyl acetate, implies that some methanol, which acts as a solute, was retained by the particles despite passage through an activated-carbon diffusion dryer. Morris et al. reported that aerosol particles generated in a nearly identical manner contained 2% methanol by weight.[6] Enhanced CCN activity[13] and increased hygroscopicity[12] of oleic acid prepared from methanol solutions have also been reported in the literature.

The activation diameter decreased from 195 to 183 nm upon exposure to 0.004 atm s of ozone. In the absence of methanol, particles were still CCN-inactive at this ozone exposure (see main text). Criegee intermediates react with alcohol functional groups to form α-alkyloxyalkyl hydroperoxides,[51] and these reaction products were present in the mass spectra of the

Aerosol CCN Properties

J. Phys. Chem. A, Vol. 111, No. 17, 2007 **3367**

TABLE 3: Pairwise Correlation Coefficients for Selected *m/z* Signal Intensities in the Mass Spectra Associated with the Data of Figure 3B[a]

m/z	81	82	85	87	93	96	97	109	111	123	124	125	141	144	152	153	155	159	171	173
81	1	–	–	–	0.813	–	–	0.91	–	–	–	–	–	–	–	–	0.863	0.752	–	0.785
82	–	1	–	–	–	0.773	–	–	–	–	–	–	–	–	–	–	–	–	–	–
85	–	–	1	–	–	–	0.747	–	–	0.806	–	0.714	–	–	–	0.751	–	–	0.829	–
87	–	–	–	1	–	–	–	–	–	–	–	–	–	–	–	–	–	–	–	–
93	0.814	–	–	–	1	–	–	0.908	–	–	–	–	–	–	–	–	0.863	0.766	–	0.863
96	–	0.773	–	–	–	1	–	–	–	–	–	–	–	–	–	–	–	–	–	–
97	–	–	0.747	–	–	–	1	–	–	0.871	–	0.95	–	–	–	0.899	–	–	–	0.751
109	0.91	–	–	–	0.908	–	–	1	–	–	–	–	–	–	–	–	0.967	0.805	–	0.874
111	–	–	–	–	–	–	–	–	1	–	–	–	–	0.804	–	–	–	–	–	–
123	–	–	0.806	–	–	–	0.871	–	–	1	–	0.865	–	–	–	0.806	–	–	0.871	–
124	–	–	–	–	–	–	–	–	–	–	1	–	–	–	0.902	–	–	–	–	–
125	–	–	0.714	–	–	–	0.95	–	–	0.865	–	1	–	–	–	0.895	–	–	–	0.774
141	–	–	–	–	–	–	–	–	–	–	–	–	1	–	–	–	–	–	–	–
144	–	–	–	–	–	–	–	–	0.804	–	–	–	–	1	–	–	–	–	–	–
152	–	–	–	–	–	–	–	–	–	–	0.902	–	–	–	1	–	–	–	–	–
153	–	–	0.751	–	–	–	0.899	–	–	0.806	–	0.895	–	–	–	1	–	–	–	0.703
155	0.863	–	–	–	0.863	–	–	0.967	–	–	–	–	–	–	–	–	1	0.82	–	0.83
159	0.753	–	–	–	0.766	–	–	0.805	–	–	–	–	–	–	–	–	0.82	1	–	0.814
171	–	–	0.829	–	–	–	–	–	–	0.871	–	–	–	–	–	–	–	–	1	–
173	0.785	–	–	–	0.863	–	0.752	0.874	–	–	–	0.774	–	–	–	0.703	0.83	0.814	–	1

[a] Dashed entries indicate that the correlation coefficient is less than 0.7.

particles (not shown). These products, however, are expected to have lower water solubility and thus be less CCN-active than methanol. We therefore hypothesize that the observed reduction in the activation diameter arises from the generation of surface-active species upon ozonolysis.

Appendix 3. Fragment Ion Analysis

As a result of high-temperature vaporization and electron-impact (EI) ionization, extensive molecular fragmentation of parent species occurs in the Q-AMS, and multiple products formed during the ozonolysis of oleic acid have the potential to form identical fragment ions. A summary of parent species and their ion fragments is given in Figure S1. Four sources of information were used to assign *m/z* values to fragment ions and their parent species, including: the EI Q-AMS mass spectra of authentic standards of AA, NN, OA, and OL;[16] the thermal-desorption particle beam mass spectrometry results of Ziemann;[21] a statistical analysis, by us, of mass spectra generated under varying exposure conditions; and standard rules of EI fragmentation.[68]

Statistical analysis of spectra collected for increasing ozone exposure allows the identification of covarying *m/z* signal intensities. Signals that covary can indicate ion fragments from the same parent species or, alternatively, molecules with identical time rates of change. Signals having low correlation coefficients can indicate ion fragments of different molecules. The correlation matrix is given in Table 3. Only *m/z* values greater than 75 and having signal-to-noise above 40 were included in the analysis.

Table 3 shows a strong correlation between *m/z* 109 and 155. Ziemann reports that the signals at 109 and 155 peaks are almost entirely due to AAHP-1.[21] Ziemann further reports that AAHP-2 is not present in high yield based on the weak intensity at *m/z* 189 peak. We believe that AAHP-2 could form initially in high yield but further react by oligomerization at its carboxylic acid group (a pathway unavailable to AAPH-1) and therefore ultimately be present at low concentration.[21] AAHP-2 may also fragment at *m/z* 109 and 155 (Figure S1), and the formation of these fragments may be favored over the formation of *m/z* 189.

Ziemann attributes the *m/z* 171 peak almost entirely to SOZ-2.[21] The increased yield of *m/z* 171 in the CCN-active particles implies that another molecule present in the CCN-active particles also fragments at *m/z* 171 because there is no source of SOZ-2 in the particles once the SCIs are consumed. The ozonolysis of the aldehyde groups of AAHP-1 and AAHP-2 to form AAHP-1* and AAHP-2*, respectively, should produce additional spectral intensity at *m/z* 171 (Figures 8 and S1). On the basis of our correlation analysis, we believe that the increase in *m/z* 127 upon activation is attributable to an increase in AAHP-1*.

Supporting Information Available: Figure S1 showing fragment ion structures consistent with the observed *m/z* values and a table of the fractional difference values corresponding to Figure 6. This material is available free of charge via the Internet at http://pubs.acs.org.

References and Notes

(1) Rudich, Y. *Chem. Rev.* **2003**, *103*, 5097.

(2) Kanakidou, M.; Seinfeld, J. H.; Pandis, S. N.; Barnes, I.; Dentener, F. J.; Facchini, M. C.; VanDingenen, R.; Ervens, B.; Nenes, A.; Nielsen, C. J.; Swietlicki, E.; Putaud, J. P.; Balkanski, Y.; Fuzzi, S.; Horth, J.; Moortgat, G. K.; Winterhalter, R.; Myhre, C. E. L.; Tsigaridis, K.; Vignati, E.; Stephanou, E. G.; Wilson, J. *Atmos. Chem. Phys.* **2005**, *5*, 1053.

(3) Koch, D. *J. Geophys. Res.* **2001**, *106*, 20311.

(4) Cooke, W. F.; Wilson, J. J. N. *J. Geophys. Res.* **1996**, *101*, 19395.

(5) Chung, S. H.; Seinfeld, J. H. *J. Geophys. Res.* **2002**, *107*, 4407.

(6) Morris, J. W.; Davidovits, P.; Jayne, J. T.; Jiminez, J. L.; Shi, Q.; Kolb, C. E.; Worsnop, D. R.; Barney, W. S.; Cass, G. *Geophys. Res. Lett.* **2002**, *29*, 1357.

(7) Moise, T.; Rudich, Y. *J. Phys. Chem. A.* **2002**, *106*, 6469.

(8) Katrib, Y.; Biskos, G.; Buseck, P. R.; Davidovits, P.; Jayne, J. T.; Mochida, M.; Wise, M. E.; Worsnop, D. R.; Martin, S. T. *J. Phys. Chem. A.* **2005**, *109*, 10910.

(9) Hearn, J. D.; Smith, G. D. *Phys. Chem. Chem. Phys.* **2005**, *7*, 2549.

(10) Thornberry, T.; Abbatt, J. P. D. *Phys. Chem. Chem. Phys.* **2004**, *6*, 84.

(11) Finlayson-Pitts, B. J.; Pitts, J. N. *Chemistry of the Upper and Lower Atmosphere: Experiments and Applications*; Academic Press: New York, 2000.

(12) Asad, A.; Mmereki, B. T.; Donaldson, D. J. *Atmos. Chem. Phys.* **2004**, *4*, 2083.

(13) Broekhuizen, K. E.; Thornberry, T.; Kumar, P. P.; Abbatt, J. P. D. *J. Geophys. Res.* **2004**, *109*, D24206.

(14) Hearn, J. D.; Lovett, A. J.; Smith, G. D. *Phys. Chem. Chem. Phys.* **2005**, *7*, 501.

(15) Hearn, J. D.; Smith, G. D. *J. Phys. Chem. A* **2004**, *108*, 10019.

(16) Katrib, Y.; Martin, S. T.; Hung, H.-M.; Rudich, Y.; Zhang, H.; Slowik, J. G.; Davidovits, P.; Jayne, J. T.; Worsnop, D. R. *J. Phys. Chem. A* **2004**, *108*, 6686.

(17) Katrib, Y.; Martin, S. T.; Rudich, Y.; Davidovits, P.; Jayne, J. T.; Worsnop, D. R. *Atmos. Chem. Phys.* **2005**, *5*, 275.

(18) Knopf, D. A.; Anthony, L. M.; Bertram, A. K. *J. Phys. Chem. A* **2005**, *109*, 5579.

(19) Reynolds, J. C.; Last, D. J.; McGillen, M.; Nijs, A.; Horn, A. B.; Percival, C.; Carpenter, L. J.; Lewis, A. C. *Environ. Sci. Technol.* **2006**, *40*, 6674.

(20) Smith, G. D.; III, E. W.; DeForest, C. L.; Baer, T.; Miller, R. E. *J. Phys. Chem. A* **2002**, *106*, 8085.

(21) Ziemann, P. J. *Faraday Discuss.* **2005**, *130*, 469.

(22) Zahardis, J.; LaFranchi, B. W.; Petrucce, G. A. *Atmos. Environ.* **2006**, *40*, 1661.

(23) Zahardis, J.; LaFranchi, B. W.; Petrucci, G. A. *J. Geophys. Res.* **2005**, *110*, D08307.

(24) Zahardis, J.; LaFranchi, B. W.; Petrucci, G. A. *Int. J. Mass Spectrom.* **2006**, *253*, 38.

(25) Zahardis, J.; Petrucci, G. A. *Atmos. Chem. Phys.* **2007**, *7*, 1237.

(26) Rudich, Y.; Donahue, N. M.; Mentel, T. F. *Annu. Rev. Phys. Chem.* **2007**, *58*, 321.

(27) Seinfeld, J. H.; Pankow, J. F. *Annu. Rev. Phys. Chem.* **2003**, *54*, 121.

(28) Altieri, K. E.; Carlton, A. G.; Kim, H.-J.; Turpin, B. J.; Seitzinger, S. P. *Environ. Sci. Technol.* **2006**, *40*, 4956.

(29) Carlton, A. G.; Turpin, B. J.; Lim, H.-J.; Altieri, K. E.; Seitzinger, S. P. *Geophys. Res. Lett.* **2006**, *33*, L06822.

(30) Lim, H.-J.; Carlton, A. G.; Turpin, B. J. *Environ. Sci. Technol.* **2005**, *39*, 4441.

(31) Vance, D. E. *Biochemistry of Lipids, Lipoproteins, and Membranes*; Elsevier: Amsterdam, 2002.

(32) Rogge, W. F.; Hildemann, L. M.; Mazurek, M. A.; Cass, G. R.; Simonelt, B. R. T. *Environ. Sci. Technol.* **1991**, *25*, 1112.

(33) Stepahanou, E. G.; Stratigakis, N. *Environ. Sci. Technol.* **1993**, *27*, 1403.

(34) Schauer, J. J.; Rogge, W. F.; Hildemann, L. M.; Mazurek, M. A.; Cass, G. R.; Simoneit, B. R. T. *Atmos. Environ.* **1996**, *30*, 3837.

(35) Hung, H.-M.; Katrib, Y.; Martin, S. T. *J. Phys. Chem. A.* **2005**, *109*, 4517.

(36) Nash, D. G.; Tolocka, M. P.; Baer, T. *Phys. Chem. Chem. Phys.* **2006**, *8*, 4486.

(37) Bailey, P. S. *Ozonation in Organic Chemistry. Volume I: Olefinic Compounds.*; Academic Press: New York, 1982; Vol. 39-I.

(38) Rader, D. J. Application of the Tandem Differential Mobility Analyzer to the Studies of Droplet Evaporation and Growth, University of Minnesota, 1985.

(39) Biskos, G.; Paulsen, D.; Russell, L. M.; Buseck, P. R.; Martin, S. T. *Atmos. Chem. Phys.* **2006**, *6*, 4633.

(40) McMurry, P. H.; Takano, H.; Anderson, G. R. *Environ. Sci. Technol.* **1983**, *17*, 347.

(41) Hearn, A. G. *Proc. Phys. Soc.* **1961**, *78*, 932.

(42) Jayne, J. T.; Leard, D. C.; Zhang, X.; Davidovits, P.; Smith, K. A.; Kolb, C. E.; Worsnop, D. R. *Aerosol Sci. Technol.* **2000**, *33*, 49−70.

(43) Jimenez, J. L.; Shi, Q.; Kolb, C. E.; Worsnop, D. R.; Yourshaw, I.; Seinfeld, J. H.; Flagan, R. C.; Zhang, X.; Smith, K. A.; Morris, J. W.; Davidovits, P. *J. Geophys. Res.* **2003**, *108*, 8425.

(44) Liu, P.; Ziemann, P. J.; Kittelson, D. B.; McMurry, P. H. *Aerosol Sci. Technol.* **1995**, *22*, 293.

(45) Liu, P.; Ziemann, P. J.; Kittelson, D. B.; McMurry, P. H. *Aerosol Sci. Technol.* **1995**, *22*, 314.

(46) Roberts, G. C.; Nenes, A. *Aerosol Sci. Technol.* **2005**, *39*, 206.

(47) Lance, S.; Meding, J.; Smith, J. N.; Nenes, A. *Aerosol Sci. Technol.* **2006**, *40*, 242.

(48) NIH toxnet database; http://toxnet.nlm.nih.gov, 2006; Vol. (accessed August 2006).

(49) Mochida, M.; Katrib, Y.; Jayne, J. T.; Worsnop, D. R.; Martin, S. T. *Atmos. Chem. Phys.* **2006**, *6*, 4851.

(50) Alfarra, M. R.; Paulsen, D.; Gysel, M.; Garforth, A. A.; Dommen, J.; Prevot, A. S. H.; Worsnop, D. R.; Baltensperger, U.; Coe, H. *Atmos. Chem. Phys.* **2006**, *6*, 7747.

(51) Bailey, P. S. *Ozonation in Organic Chemistry. Volume II: Non-olefinic Compounds.*; Academic Press: New York, 1982; Vol. 39-II.

(52) Story, P. R.; Alford, J. A.; Burgess, J. R.; Ray, W. C. *J. Am. Chem. Soc.* **1971**, *93*, 3042.

(53) White, H. M.; Bailey, P. S. *J. Org. Chem.* **1965**, *30*, 3037.

(54) Erickson, R. E.; Bakalik, D.; Richards, C.; Scanlon, M.; Huddleston, G. *J. Org. Chem.* **1965**, *31*, 461.

(55) Marcolli, C.; Canagaratna, M. R.; Worsnop, D. R.; Bahreini, R.; deGouw, J. A.; Warneke, C.; Goldan, P. D.; Kuster, W. C.; Wiliams, E. J.; Lerner, B. M.; Roberts, J. M.; Meagher, J. F.; Fehsenfeld, F. C.; Marchewka, M. L.; Bertman, S. B.; Middlebrook, A. M. *Atmos. Chem. Phys.* **2006**, *6*, 5649.

(56) Zhang, Q.; Canagaratna, M. R.; Jayne, J. T.; Worsnop, D. R.; Jimenez, J.-L. *J. Geophys. Res.* **2005**, *110*, D070S9.

(57) Alfarra, M. R.; Coe, H.; Allan, J. D.; Bower, K. N.; Boudries, H.; Canagaratna, M. R.; Jimenez, J. L.; Jayne, J. T.; Garforth, A. A.; Li, S.; Worsnop, D. R. *Atmos. Environ.* **2004**, *38*, 5745.

(58) Raymond, T. M.; Pandis, S. N. *J. Geophys. Res.* **2003**, *108*, 4469.

(59) Broekhuizen, K.; Kumar, P. P.; Abbatt, J. P. D. *Geophys. Res. Lett.* **2004**, *31*, Article L01107.

(60) Abbatt, J. P. D.; Broekhuizen, K.; Kumar, P. *Atmos. Environ.* **2005**, *39*, 4767.

(61) Saxena, P.; Hildemann, L. M. *J. Atmos. Chem.* **1996**, *24*, 57.

(62) Rogge, W. F.; Mazurek, M. A.; Hildemann, L. M.; Cass, G. R.; Simoneit, B. R. T. *Atmos. Environ.* **1993**, *27A*, 1309.

(63) Brechtel, F. J.; Kreidenweis, S. M. *J. Atmos. Sci.* **2000**, *57*, 1854.

(64) Pitzer, K. S.; Mayorga, G. *J. Phys. Chem.* **1973**, *77*, 2300.

(65) Skoog, D. A.; Holler, F. J.; Nieman, T. A. *Principles of Instrumental Analysis*, 5th ed.; Harcourt Brace College Publishers: Philadelphia, PA, 1998.

(66) Biskos, G.; Russell, L. M.; Buseck, P. R.; Martin, S. T. *Geophys. Res. Lett.* **2006**, *33*, L07801.

(67) Kinney, P. D.; Pui, D. Y. H.; Mulholland, G. W.; Bryner, N. P. *J. Res. Natl. Inst. Stand. Technol.* **1991**, *96*, 147.

(68) McLafferty, F. W.; Turecek, F. *Interpretation of Mass Spectra*, 4th ed.; University Science Books: Sausalito, CA, 1993.

(69) Kreidenweis, S. M.; Koehler, K.; DeMott, P. J.; Prenni, A. J.; Carrico, C.; Ervens, B. *Atmos. Chem. Phys.* **2005**, *5*, 1357.